

Manuscript version: Author's Accepted Manuscript

The version presented in WRAP is the author's accepted manuscript and may differ from the published version or Version of Record.

Persistent WRAP URL:

<http://wrap.warwick.ac.uk/175742>

How to cite:

Please refer to published version for the most recent bibliographic citation information. If a published version is known of, the repository item page linked to above, will contain details on accessing it.

Copyright and reuse:

The Warwick Research Archive Portal (WRAP) makes this work by researchers of the University of Warwick available open access under the following conditions.

Copyright © and all moral rights to the version of the paper presented here belong to the individual author(s) and/or other copyright owners. To the extent reasonable and practicable the material made available in WRAP has been checked for eligibility before being made available.

Copies of full items can be used for personal research or study, educational, or not-for-profit purposes without prior permission or charge. Provided that the authors, title and full bibliographic details are credited, a hyperlink and/or URL is given for the original metadata page and the content is not changed in any way.

Publisher's statement:

Please refer to the repository item page, publisher's statement section, for further information.

For more information, please contact the WRAP Team at: wrap@warwick.ac.uk.

Application of Unsupervised Learning in Implementation of Joint Power and Index Modulation Access in V2X Systems

Sunyoung Lee, Konstantinos Koufos, Carsten Maple and Mehrdad Dianati

Abstract—The implementation of joint Power-and-Index Modulation Access (PIMA), which is an effective way of realizing non-orthogonal multiple access (NOMA), requires a process of user ordering over the available subcarriers, before multiplexing their data streams for power and index modulation. The conventional way of user ordering in NOMA with respect to the channel state information can be impractical and expensive given the large numbers of users and subcarriers, in Vehicle-to-Everything (V2X) communications. Therefore, this paper proposes a novel approach that leverages K-Means clustering to learn the pattern of multi-user multi-carrier energy variations and use them to effectively order the users. For this, we develop several learning algorithms and an analytical model for the Symbol Error Probability (SEP) of PIMA, which is used to quickly generate part of the training dataset (transfer learning). The results of the comprehensive evaluations that have been carried out in this study show that the proposed approach outperforms the benchmark techniques in terms of SEP. It is also shown that the proposed scheme provides improved performance in terms of SEP as compared to distance-based ordering in realistic V2X scenarios using synthetic mobility traces for the locations of vehicles along multi-lane highways.

Index Terms—Index Modulation (IM), K-Means clustering, mobility traces, non-orthogonal multiple access (NOMA), Vehicle-to-Everything (V2X).

I. INTRODUCTION

Vehicle-to-Everything (V2X) communications demand high-reliability and low-latency wireless connectivity for the purpose of safety-related functions, while for entertainment and infotainment services, enhanced mobile broadband connections become relevant. Therefore, it is important to design a spectrum-efficient multiple access scheme for a large number of connected vehicles in V2X systems. In this context, Non-Orthogonal Multiple Access (NOMA) technique for V2X communication has recently become increasingly attractive [1]–[4].

In NOMA [5]–[8], the spectral efficiency can be enhanced by multiplexing the data streams of different users over the same time-frequency resource blocks using different power levels. Recently, Index Modulation (IM) [9]–[11] has been also considered for improving the spectral efficiency and reliability

of Orthogonal Frequency Division Multiplexing (OFDM) technique. The main idea behind IM is to activate a subset of subcarriers and use their indices to convey additional information. There are various ways that IM can be implemented within the NOMA framework [12]–[15]. A promising approach is to use IM in conjunction with power-domain multiplexing dubbed as the joint Power-and-Index Modulation Access (PIMA). This technique has particularly attracted interest for downlink communication in V2X applications [16].

In PIMA, the Base Station (BS) needs to order the users before multiplexing their data streams for index and power modulation. The selected ordering depends on the channel quality. Specifically, the information of the user with the worst channel conditions is modulated on the indices of the activated subcarriers, while the rest of the users are multiplexed onto the same subcarriers with different power levels [16]. The users can decode their own data via Successive Interference Cancellation (SIC) that is often used to cancel multi-user interference. As a result, in PIMA/NOMA, the quality of user ordering directly affects the performance of the entire system. Therefore, an effective user ordering is an important and non-trivial technical challenge in such systems.

There are two widely-used approaches in the literature to identify the best user ordering for NOMA. In the first one, the BS exploits the instantaneous Channel State Information (CSI). This can be achieved by users estimating their downlink CSIs and reporting them back to the BS. Alternatively, in Time Division Duplexing (TDD) systems, the BS can estimate the downlink CSI from the uplink CSI measurements assuming the reciprocity of the uplink and downlink channels. This means that the BS requires the CSIs from all users every Transmit Time Interval (TTI) for the user ordering task, which is expensive and impractical for V2X systems, where the channel varies quite rapidly [4], [17], [18].

In the second approach, the BS orders the users according to their distances [13]–[15], [19]–[21]. This approach cannot accurately capture the real channel state in complex environments with non-line-of-sight propagation conditions. Moreover, the ordering of users may vary across sub-carriers in multi-carrier systems experiencing frequency selective fading. This makes the user ordering in PIMA/NOMA implementations even more challenging and resource-expensive.

Unfortunately, the ordering complexity in PIMA/NOMA increases with the number of users, possibly imposing a heavy measurement and computational load at the BS. For example, with L users and N subcarriers, the computational complexity

A preliminary part of this paper was presented at the *IEEE VTC Spring*, 2020. This work was supported by Jaguar Land Rover and the UK-EP SRC grant EP/N01300X/1 as part of the jointly funded Towards Autonomy: Smart and Connected Control (TASCC) Programme.

S. Lee, K. Koufos, C. Maple and M. Dianati are with Warwick Manufacturing Group, University of Warwick, Coventry, CV4 7AL, U.K. (email: {sunyoung.lee, Konstantinos.Koufos, CM, m.dianati}@warwick.ac.uk).

of the ordering is $(L \times N)!$. This becomes a significant challenge in V2X systems, where the low latency requirements render computationally expensive ordering algorithms non-effective. Therefore, there is a need for efficient methods for user ordering in PIMA/NOMA for V2X systems [1]–[4], [16], which strike an acceptable balance between the quality and the complexity of the ordering algorithm.

Recent reviews of the ordering approaches for NOMA can be found in [1] and [22]–[24], but they are tailored to single-carrier communication systems. In [1], the authors consider partial CSI for power-domain multiplexing in NOMA that contains only the effects of path loss and shadowing. The coverage probability of NOMA with user ordering based on the instantaneous channel power gain is studied in [22], while distance-based ordering is examined in [23]. Finally, a comparative analysis of Signal-to-Interference and Noise Ratio (SINR)-based coverage probability using the distance-based and the instantaneous CSI-based user ordering for two static NOMA users is studied in [24]. Unfortunately, the distance-based approach for user ordering cannot accurately capture the real channel state in complex environments, and the CSI-based approach is expensive and impractical for V2X systems. More importantly, both approaches are not straightforward to extend to multi-carrier systems. Judging by such shortcomings and gaps, an effective user ordering scheme for multi-carrier NOMA V2X systems is still in its infancy.

Motivated by the aforementioned challenges and needs, this paper proposes to learn the patterns of multi-user multi-carrier energy variations in the uplink and use them to effectively order the users for PIMA. The reliance of the ordering task on complicated channel estimation techniques at every TTI is therefore alleviated. That significantly reduces the implementation complexity and allows the BS to effectively order the users in real-time. It has been a common practice to employ machine learning tools for obtaining in real-time the solution to computationally-expensive problems. In this article, we show how to order the users in PIMA using a bespoke K-Means clustering algorithm. The suggested algorithm uses the standard K-means to cluster together similar vectors of uplink signal energies during training. Afterward, the optimal user order for the centroid of each cluster is identified. Finally, during real-time inference, the observed vector of signal energies in the uplink is associated with the nearest centroid and the optimal user order can be retrieved.

The motivation for selecting K-Means clustering among various other learning algorithms, e.g., artificial neural networks, is its simplicity and low-storage requirements. The BS can simply store and use the cluster centroids to obtain the best user ordering during real-time inference. Despite its simplicity, K-Means yields significant performance gains in comparison with the benchmarking schemes for user ordering, as it will be illustrated later in this article. Furthermore, K-Means provides an intuitive justification for the adoption of machine learning in the subject problem, because it is natural to assume that similar vectors of received signal energies in the uplink would lie within the same cluster and be associated with the same best ordering of vehicles. The main contributions of this work are summarized next.

- A novel approach is proposed where the BS learns to estimate an effective user order given the instantaneous received energies across subcarriers and users in the uplink. Complicated channel estimation techniques involving, for instance, matrix inversions are therefore avoided. To achieve an ordering that yields a low Symbol Error Probability (SEP), we consider several ordering selection rules, e.g., Min-Avg, Min-Max, and Min-Min.
- To reduce the training complexity, the idea of model-based machine learning [25], [26] is adopted. Specifically, a closed-form approximation is derived for the SEP performance of PIMA, which helps to quickly generate part of the training dataset (transfer learning). Note that as compared to our previous work in [16], we have generalized the system model with respect to the number of vehicles and subcarriers.
- To track the required number of clusters, the cross-validated K-Means algorithm is investigated, and to further reduce the training time, the performance of mini-batch K-Means clustering [27]–[29] is analyzed.
- Finally, to corroborate the applicability of our scheme in realistic V2X settings, we validate its performance using mobility traces for the locations (and hence the path-loss) of vehicles along multi-lane motorways [30]–[33].

The rest of this paper is organized as follows. The system model and key assumptions are specified in Section II. Section III describes the structure of the proposed learning-driven PIMA and the learning algorithm, followed by Mini-batch K-Means clustering and the cross-validation algorithm for our model. Section IV describes the process of real-time estimation to obtain an effective ordering. The simulation results are presented and discussed in Section V, followed by the conclusions in Section VI.

Notations: Uppercase and lowercase bold-faced letters indicate matrices and vectors, respectively. $(\cdot)^T$ and $\mathbb{E}[\cdot]$ represent transpose and expectation, respectively. $\mathcal{CN}(\mathbf{w}, R)$ represents the distribution of a complex Gaussian random variable with mean \mathbf{w} and covariance R . (\cdot) and $\lfloor \cdot \rfloor$ represent the binomial coefficient and the floor function, respectively. $\|\cdot\|_F$ stands for the Frobenius norm.

II. SYSTEM MODEL

We consider a downlink multiple access multi-carrier V2X communication system, where the BS uses joint power and index modulation to send data signals to L vehicles in TDD-based mode. To multiplex their data across the active subcarriers and their indices, the BS must first learn to order the vehicles based on their channel conditions. Therefore, the BS comprises three functional components: (i) off-line training with dynamic patterns of ordering vehicles (or users) to learn an effective ordering strategy; (ii) real-time estimation of the user order; and (iii) PIMA signal generation given the user order, see Fig. 1. Every vehicle needs to know its order within the PIMA scheme, which is communicated from the BS by exploiting the insertion of pilot sequences in the beginning of each transmission block. For the sake of simplicity, a single antenna scenario is considered.

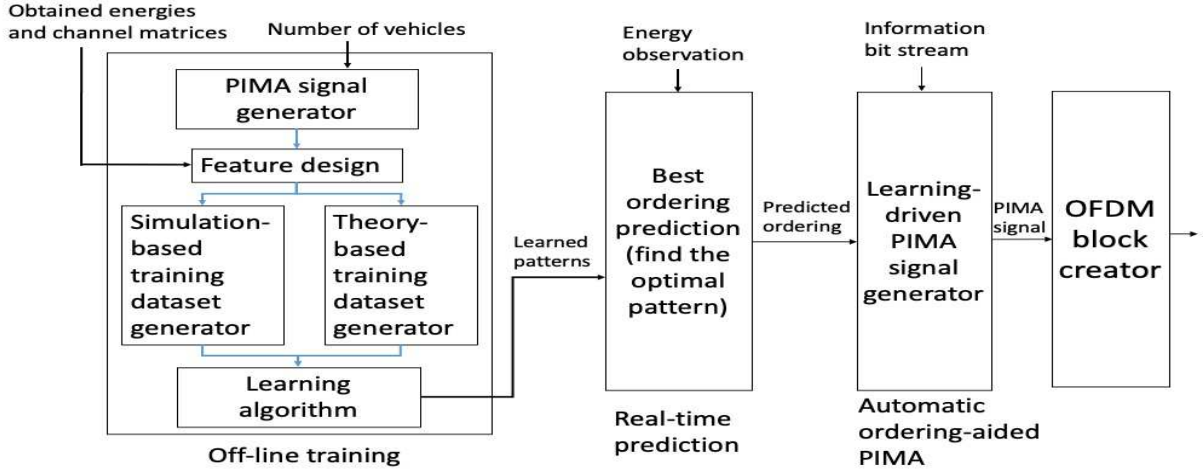


Fig. 1: System structure with offline training and learning-driven multiple access.

TABLE I: Table of notations.

Notation	Description
L	Number of vehicles
N_t	Number of total subcarriers
N	Number of subcarriers within a block
G	Number of blocks
k	Number of active subcarriers within a block
P_t	Average total transmit power of each subcarrier
$\bar{\rho}_l$	Average SNR per subcarrier at V_l
a_l	Power allocation factor for V_l
m_l	Information bit stream of V_l
\tilde{m}_l	Number of bits per symbol for V_l
\mathbf{H}_l	Channel matrix at V_l
h_{ln}	Channel coefficient of subcarrier n at V_l
\mathbf{w}_n	Weight vector
$\Theta_l, \theta_{nf,l}$	Doppler parameters at V_l
ϵ_l	Normalized Doppler spread at V_l
\mathcal{S}	Constellation at $V_l, 1 \leq l \leq L-1$
s_l	Complex data symbol
$x_{\mathcal{I}}$	IM symbol
R	Number of training data points
K_c	Number of clusters in K-Means clustering
\mathbf{e}_r	The r -th energy vector during training
\mathbf{q}_u	The u -th cluster's centroid

Concerning the communication link model, the BS non-orthogonally multiplexes bit streams for L vehicles onto N_t subcarriers. In the standards for OFDM-based V2X communication, N_t is usually a power of two, i.e., $N_t = 2^W$ for an integer $W \geq 2$. Without loss of generality, we group every $N = 4$ consecutive subcarriers together, i.e., $N_t = NG$, where G is the number of groups. Each group is treated independently of others and thus, we hereafter focus on a single group. The incoming information bit stream at the BS is mapped to an $N \times 1$ vector denoted by \mathbf{x} . The vector $\mathbf{x} = [x_1, \dots, x_N]^T$ represents the transmit signal vector in the frequency domain, with x_n for $n = 1, \dots, N$ being the modulated PIMA signal on the n -th subcarrier. To generate \mathbf{x} , the BS activates $k = 2$ out of the total $N = 4$ subcarriers such that $\|\mathbf{x}\|_0 = k$, while the rest $(N - k)$ subcarriers are zero padded. The active subcarriers contain superpositioned signals for the vehicles employing NOMA. Denote by V_l the l -th vehicle for $l = 1, \dots, L$. The vehicles V_1 and V_L are referred to as the vehicles with the best and the worst channel conditions, respectively, while the rest ($V_l, l = 2, \dots, L - 1$)

are referred to as the vehicles under mild channel conditions. The channel gains on the n -th subcarrier can be sorted as $|h_{n1}|^2 \geq |h_{n2}|^2 \geq \dots \geq |h_{nL}|^2$, where $|h_{nl}|^2$ denotes the channel power gain on the n -th subcarrier for the vehicle V_l . Note that the ordering of vehicles based on their channel power gains may vary across the subcarriers due to frequency selectivity. Making an efficient decision on the vehicle ordering for multi-carrier systems is therefore challenging, and will be discussed in detail in Section III.

A. Generation of PIMA signals with L vehicles

Next, we describe the process of creating the PIMA transmit signal vector \mathbf{x} given the ordering of vehicles. This process consists of two parts: Index Modulation (IM) and superposition modulation. In the IM part, the bit stream of the vehicle with the worst channel conditions, V_L , is denoted by m_L , and is modulated on the indices of active subcarriers, see Fig. 2. In the superposition part, the bit streams of the other vehicles, m_l for $l = 1, \dots, L - 1$, are modulated jointly onto the power and subcarriers of the active indices. The bit stream of V_1 is modulated on all active subcarriers using repetition coding because, as we will shortly explain, the power allocated to V_1 would be actually the smallest, and thus, frequency diversity is used to enhance the symbol detection performance for V_1 .

1) *Index Modulation:* A combination of indices of the active subcarriers is referred to as the IM symbol, which is denoted by $x_{\mathcal{I}} = \{i_1, \dots, i_k\}$, where $i_\nu \in \{1, \dots, N\}$, $\nu = 1, \dots, k$. The total number of $x_{\mathcal{I}}$ symbols is $\binom{N}{k}$, and thus, the number of bits per symbol is at most $\lfloor \log_2 \binom{N}{k} \rfloor$. Given the symbol $x_{\mathcal{I}}$, the BS may generate the matrix $\mathbf{W} = [\mathbf{w}_1, \dots, \mathbf{w}_k]$, where \mathbf{w}_ν is an $N \times 1$ zero vector except the i_ν -th element being equal to one. See also Table I for the list of most important notations used in this paper. Apparently, there exists a trade-off between the spectral efficiency and transmit diversity in the IM part. The use of orthogonal combinations of active indices (orthogonal IM symbols) can produce higher diversity gain at the cost of reduced number of transmitted bits per IM symbol. Taking into account this trade-off, we consider orthogonal IM symbols for PIMA to prevent

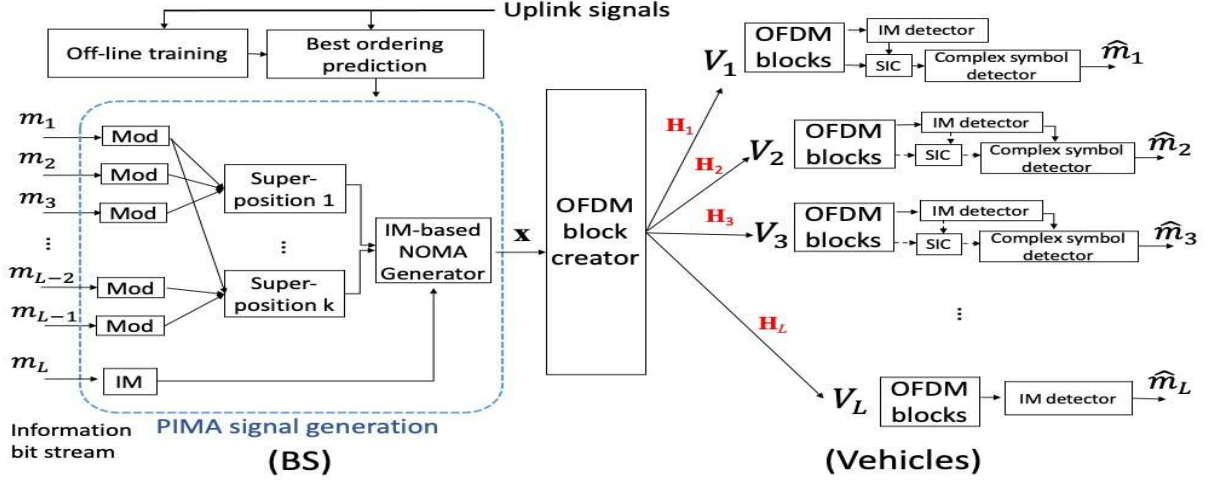


Fig. 2: Communication system structure of PIMA scheme with L vehicles.

interference between IM symbols. In PIMA implementation, the number of orthogonal IM symbols is $N_{\mathcal{I}} = \lfloor \frac{N}{k} \rfloor$. Apart from the gain due to diversity, the use of orthogonal IM symbols also reduces the computational complexity of the maximum-likelihood (ML) detection in PIMA receivers, as compared to ML detection in the standard IM implementation, see for instance [10, Eq. (10)].

The generation of PIMA signals for $N = 4$ subcarriers with $k = 2$ activated subcarriers is summarized in Table II. We consider two possible generated symbols, $N_{\mathcal{I}} = 2$, hence the number of transmitted information bits per symbol in the IM part is equal to one. We activate non-adjacent subcarriers within an IM symbol, e.g., '1' and '3', or '2' and '4' for better robustness to Inter Carrier Interference (ICI). Finally, $x_{\mathcal{I}} \in \{\mathcal{I}_1, \mathcal{I}_2\}$, where $\mathcal{I}_1 = \{1, 3\}$, $\mathcal{I}_2 = \{2, 4\}$.

2) *Superposition Modulation*: Once the IM symbol $x_{\mathcal{I}}$ is selected, the corresponding subcarriers are modulated to convey the information bit streams for the rest of the vehicles. For this, let $s_l \in \mathcal{S}$ be the complex data symbol for the vehicle V_l , $l = 1, \dots, L-1$ with $\mathbb{E}\{s_l\} = 0$, $\mathbb{E}|s_l|^2 = 1$, and let \mathcal{S} denote the constellation set, which is common for all these vehicles. Denote by $\tilde{\mathbf{x}}_l$ the modulated signal for V_l . Recall that for V_1 , repetition coding is used, and thus, for $k = 2$, we have $\tilde{\mathbf{x}}_1 = \sqrt{P_t N/k} [s_1, s_1]^T$, where P_t denotes the average transmit power of each subcarrier. Additionally, every vehicle V_l , $2 \leq l \leq L-1$ is modulated on a single activated subcarrier, i.e., for $k = 2$, $\tilde{\mathbf{x}}_l = \sqrt{P_t N/k} [s_l, 0]^T$, for an even $l < L$, denoted by l_e , and $\tilde{\mathbf{x}}_l = \sqrt{P_t N/k} [0, s_l]^T$, for an odd $\{l : l \leq L-1, l \notin \{1\}\}$, denoted by l_o . The accumulated information bits conveyed by $\tilde{\mathbf{x}}_l$, $1 \leq l \leq L-1$ are $\sum_{l=1}^{L-1} \tilde{m}_l = (L-1) \log_2 |\mathcal{S}|$ bits, where $|\mathcal{S}|$ is the cardinality of \mathcal{S} , but the total transmitted bits are $L \log_2 |\mathcal{S}|$ because repetition coding is used for the symbol of V_1 .

3) *PIMA signals*: With the transmitted signal vectors for each vehicle at hand, the PIMA signal generator can finally superpose the information bits of vehicles V_l , $l = 1, \dots, L-1$ onto the k active subcarriers using different power levels. In particular, an $N \times 1$ vector mapped for the bit stream m_l of V_l is generated as $\mathbf{x}_l = a_l \mathbf{W} \tilde{\mathbf{x}}_l$, where a_l^2 is the power

TABLE II: Example PIMA signal generation for a block of $N = 4$ subcarriers with $k = 2$ activated subcarriers.

IM signal ($x_{\mathcal{I}}$)	Super-positioned signals ($x = x_{i_1}, \bar{x} = x_{i_2}$)	PIMA signal (\mathbf{x})
$\mathcal{I}_1 = \{1, 3\}$	$x = \sqrt{P_t N k^{-1}} (a_1 s_1 + \sum_{l \in \mathcal{I}_1} a_l s_l)$	$\mathbf{x} = [x, 0, \bar{x}, 0]^T$
$\mathcal{I}_2 = \{2, 4\}$	$\bar{x} = \sqrt{P_t N k^{-1}} (a_1 s_1 + \sum_{l \in \mathcal{I}_2} a_l s_l)$	$\mathbf{x} = [0, x, 0, \bar{x}]^T$

allocation for V_l , which satisfies $a_1^2 + \sum_{l \in \mathcal{I}_e} a_l^2 = 1$ with $a_1^2 < a_2^2 < a_4^2 < \dots < a_{L-2}^2$, and $a_1^2 + \sum_{l \in \mathcal{I}_o} a_l^2 = 1$ with $a_1^2 < a_3^2 < a_5^2 < \dots < a_{L-1}^2$ for an even number L of vehicles. That is, for vehicle V_1 , we have $\mathbf{x}_1 = a_1 \mathbf{W} \tilde{\mathbf{x}}_1$, where the non-zero elements of the vector \mathbf{x}_1 are the indices of activated subcarriers. For example, when $x_{\mathcal{I}} = \mathcal{I}_1 = \{1, 3\}$, we can have $\mathbf{x}_1 = a_1 \mathbf{W} \tilde{\mathbf{x}}_1 = a_1 \sqrt{P_t N k^{-1}} [s_1, 0, s_1, 0]^T$, where $N k^{-1} = 2$ is used to normalize the power, and $\mathbf{W} = [\mathbf{w}_1, \mathbf{w}_2]$ with $\mathbf{w}_1 = [1, 0, 0, 0]^T$ and $\mathbf{w}_2 = [0, 0, 1, 0]^T$.

Similarly, the $N \times 1$ vector \mathbf{x}_l for the vehicles V_l , $2 \leq l \leq L-1$, can be modulated onto one of the active subcarriers. When $x_{\mathcal{I}} = \mathcal{I}_1 = \{1, 3\}$, for the vehicles with an even index $l \in l_e$, the modulated signal is $\mathbf{x}_l = a_l \mathbf{W} \tilde{\mathbf{x}}_l = a_l \sqrt{P_t N k^{-1}} [s_l, 0, 0, 0]^T$, and similarly, for the vehicles with an odd index, $l \in l_o$, we have $\mathbf{x}_l = a_l \mathbf{W} \tilde{\mathbf{x}}_l = a_l \sqrt{P_t N k^{-1}} [0, 0, s_l, 0]^T$. Eventually, x and \bar{x} denote the super-positioned signals of vehicles V_l , $1 \leq l \leq L-1$ modulated onto the active subcarriers, and $P_t (= 1)$ is the normalized transmit power level. Finally, the transmit vector of the overall PIMA signal can be represented as

$$\mathbf{x} = \sum_{l=1}^{L-1} \mathbf{x}_l = \sum_{l=1}^{L-1} a_l \mathbf{W} \tilde{\mathbf{x}}_l. \quad (1)$$

It is noteworthy that $\|\mathbf{x}_1\|_0 = k > \|\mathbf{x}_l\|_0 = 1$ for $2 \leq l \leq L-1$, $\mathbb{E}\|\mathbf{x}_1\|^2 = a_1^2 P_t N$ and $\mathbb{E}\|\mathbf{x}_l\|^2 = a_l^2 P_t N/k$. Note that the bits m_l , $1 \leq l \leq L-1$ are modulated jointly onto the power and subcarrier index domains.

B. Signal detection model at the vehicles

In the downlink, Doppler spread is also considered to capture the effect of user mobility on V2X received signals,

using the frequency-domain response developed in [34], [35]. The received signal vector at the vehicle V_l (in the frequency domain) can be expressed as

$$\mathbf{y}_l = \sqrt{\bar{\rho}_l} \check{\mathbf{H}}_l \sum_{l=1}^{L-1} \mathbf{x}_l + \mathbf{n}_l, \quad (2)$$

where $\bar{\rho}_l$ is the average Signal-to-Noise Ratio (SNR) per subcarrier, $\mathbf{n}_l \sim \mathcal{CN}(\mathbf{0}, \mathbf{I}_N)$ is the additive white Gaussian noise vector with \mathbf{I}_N being the $N \times N$ identity matrix, and the derivation of the matrix $\check{\mathbf{H}}_l = \check{\Theta}_l \mathbf{H}_l$ is explained below.

The diagonal matrix $\mathbf{H}_l = \text{diag}(h_{l1}, \dots, h_{lN})$ is the channel matrix (CSI) at V_l across the N subcarriers, where the element h_{ln} follows the complex-valued Gaussian distribution with zero mean and unit variance, i.e., $h_{ln} \sim \mathcal{CN}(0, 1)$ ¹. The square matrix $\check{\Theta}_l$ is the correlation matrix with the element $\theta_{nf,l}$ representing the ICI between the n -th and the f -th subcarriers. The parameter $\theta_{nf,l}$ at V_l depends on the channel frequency offset and is given by [35, Eq. (2)]: $\theta_{nf,l} =$

$$\frac{\sin(\pi(n-f+\epsilon_l))}{N \sin \frac{\pi}{N}(n-f+\epsilon_l)} \exp \left[j\pi \left(1 - \frac{1}{N}\right)(n-f+\epsilon_l) \right], \quad (3)$$

where ϵ_l is the l -th vehicle's normalized Doppler spread, which is defined as the ratio of the Doppler frequency spread to the subcarrier frequency spacing. When the normalized Doppler spread goes to zero, the off-diagonal elements $\theta_{nf,l}$ become zero too and $\check{\Theta}_l$ degenerates to an identity matrix.

In equation (2), the received signal vector can be separated into the ideal channel term, \mathbf{H}_l , and the ICI term $\check{\Theta}_l$. Accordingly, the received signal y_{ln} on the n -th subcarrier can be written as [35, Eq. (1)]

$$y_{ln} = \sqrt{\bar{\rho}_l} h_{ln} x_{ln} + \sqrt{\bar{\rho}_l} \sum_{f=1, f \neq n}^N \theta_{nf,l} x_{lf} + n_{ln}, \quad (4)$$

where h_{ln} and n_{ln} are the channel coefficient and the noise, respectively. The x_{ln} and x_{lf} are the super-positioned signals on the n -th and the f -th subcarrier, respectively. The second term in equation (4) is the ICI term caused by the Doppler frequency spread.

Based on equations (2)-(4) and employing a maximum likelihood (ML) detector, each vehicle can detect its symbols. **It shall be noted that the use of orthogonal IM symbols reduces the computational complexity of ML detection in PIMA receivers, in comparison with ML detection in standard IM [10, Eq. (10)]. For instance, for N_t subcarriers and $k = N_t/2$, the number of symbols in standard IM is $2^{\lceil \log_2 C(N_t, N_t/2) \rceil} \geq 2^{\lfloor N_t/2 \rfloor}$. In our case, where $N = 4$ and $k = 2$, we have only two IM symbols per group of subcarriers. Then we have to repeat the same procedure for $G = N_t/N$ groups of subcarriers. Therefore the computational complexity in the number of subcarriers turns from exponential to linear.**

¹It is straightforward to generalize this channel model to include different median propagation path-loss for the vehicles. This has been omitted here to simplify the notation but it will be taken into account in the numerical illustrations in Section V.

III. OFF-LINE TRAINING MODEL

In this section, we consider a learning-based model for getting the best orderings of vehicles in PIMA. To do that the BS learns the relationship between the received signal energies in the uplink and the SEPs for the vehicles. Next, we show how to generate the training dataset and discuss several selection rules on the feature design.

A. Training dataset generation model

Let us consider a training dataset of R points, $\{\check{\mathbf{e}}_r\}_{r=1}^R$, where $\check{\mathbf{e}}_r$ is the r -th point of the set. We define $\check{\mathbf{e}}_r = \{\mathbf{e}_r, C_r^*\}$, where $\mathbf{e}_r = [\{\{|\check{y}_{l,n,r}|^2\}_{n=1}^N\}_{l=1}^L]$ is a column vector with $L \times N$ elements and the integer C_r^* is an indicator for the best ordering of vehicles. The element $\check{y}_{l,n,r}$ denotes the r -th uplink signal at the BS on the n -th subcarrier due to transmissions originated from the vehicle V_l . The BS can obtain the received signal energy, $|\check{y}_{l,n,r}|^2$, using the well-developed multi-carrier sensing schemes [36]–[38]. Afterward, the BS can scale the measured energies $|\check{y}_{l,n,r}|^2$ by the transmit power level per user and subcarrier, which is a realistic assumption under uplink closed-loop power control. During training, the BS also needs to estimate the uplink CSI, $\check{\mathbf{H}}_r$, and from that obtain the downlink CSI $\check{\mathbf{H}}_l$ assuming channel reciprocity, which is required to evaluate the SEPs for the vehicles.

To compute the best ordering of vehicles, C_r^* , given the vector of uplink signal energies \mathbf{e}_r , we must consider all possible orderings. Let us denote them by $C_j, j = 1, 2, \dots, J$, where $J = L(L-1)$. Recall that we consider three types of vehicles in the system model, i.e., one vehicle with the best channel condition, another with the worst channel condition and all remaining vehicles are grouped together under mild channel conditions yielding J possible orderings. In order to compute the order C_r^* , we need a selection rule which is discussed next.

B. Selection rules

Given the user order C_j and the uplink signal energies \mathbf{e}_r , we denote by $\mathbf{P}_{j,l,r}$ the SEP of $V_l, l = 1, \dots, L$ associated with the r -th point of the training dataset. To find the best order C_r^* , the BS needs to evaluate the SEPs for all vehicles and for all orders of vehicles. Once the SEPs are calculated, $\{\{\mathbf{P}_{j,l,r}\}_{l=1}^L\}_{j=1}^J$, the BS compares them, in order to select the best order C_r^* , as the one satisfying one of the following selection rules: R1. Min-Max selection; R2. Min-Avg selection; R3. Min-Min selection. Specifically,

$$\begin{aligned} R1: C_r^* &= \arg \min_j (\max_l \{\mathbf{P}_{j,l,r}\}). \\ R2: C_r^* &= \arg \min_j (\text{avg}_l \{\mathbf{P}_{j,l,r}\}). \\ R3: C_r^* &= \arg \min_j (\min_l \{\mathbf{P}_{j,l,r}\}). \end{aligned} \quad (5)$$

It is noteworthy that the BS uses an exhaustive search to find the best order $C_r^*, \forall r$ by solving the optimization problem in Eq. (5) only during offline training. For real-time inference, the BS does not consume any extra resources for numerical optimization, as it can simply use the learned centroids.

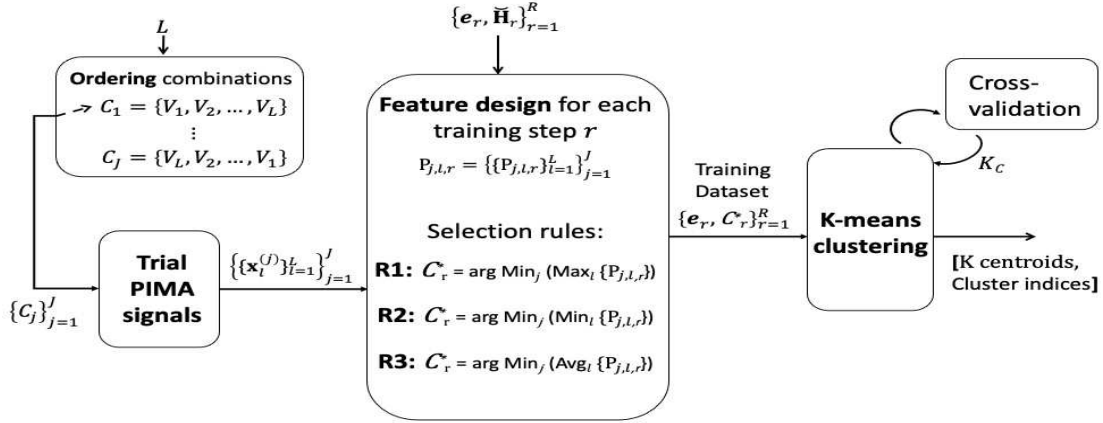


Fig. 3: Off-line training for learning-driven PIMA with K-Means clustering.

C. Bespoke K-means learning algorithm

In K-Means clustering only the locations of the centroids need to be computed and stored. In our case, each centroid is a point in the \$(L \times N)\$-dimensional space. Initially, the locations of the centroids are randomly chosen. Then, each member of the training dataset \$\{e_r\}_{r=1}^R\$ is assigned to the nearest centroid in terms of Euclidean distance, and the index of the nearest cluster is given by

$$u_r = \arg \min_u \|\mathbf{q}_{u,t} - \mathbf{e}_r\|_2, \text{ for } u = 1, \dots, K_c, \quad (6)$$

where \$K_c\$ is the number of centroids, \$\mathbf{q}_{u,t}\$ denotes the location of the \$u\$-th centroid at iteration \$t\$, and \$u_r \in \{1, 2, \dots, K_c\}\$ is the index of the nearest centroid to the dataset point \$\mathbf{e}_r\$. Once each dataset point is associated with a centroid, the locations of the centroids are iteratively updated as the average of their members:

$$\mathbf{q}_{u,t} = \frac{\sum_r \delta_{u_r,u} \mathbf{e}_r}{\sum_r \delta_{u_r,u}}, \text{ for iteration } t \geq 1, \forall u, \quad (7)$$

where \$\delta_{x,y}\$ is the Kronecker delta function.

Algorithm 1 Bespoke K-Means clustering algorithm for generating the training dataset in PIMA

- 1: Initialization: Select \$K_c, t = 0\$.
- 2: Input: \$\{e_r, C_r^*\}_{r=1}^R\$ training dataset based on one of the selection rules (R1, R2, or R3).
- 3: Initialize randomly the cluster centroids.
- 4: **repeat**
- 5: \$\{e_r\}_{r=1}^R\$ are assigned to the nearest centroid, referring to equation (6).
- 6: Update \$\mathbf{q}_{u,t}\$ as the average of members in cluster \$u\$ at iteration \$t\$, referring to equation (7).
- 7: \$t = t + 1\$.
- 8: **until** \$t = T\$ (the centroids no longer change).
- 9: Output: \$[\{\mathbf{q}_{u,T}\}_{u=1}^{K_c}, \{u_r\}_{r=1}^R]\$
- 10: Calc.: \$C_u^* = \text{majority} \{C_r^*\}_{r:u_r \in u}\$, for \$u = 1, \dots, K_c\$.

The iterations continue until the change in the centroids becomes less than a predefined threshold. After that, the

algorithm returns (i) the centroids \$\{\mathbf{q}_{u,T}\}_{u=1}^{K_c}\$, where \$T\$ counts the required number of iterations, and (ii) the cluster indices \$u_r\$ for each dataset point. Hereafter, we will omit the subscript \$T\$ for brevity hence, \$\mathbf{q}_{u,T} \equiv \mathbf{q}_u\$. Finally, one more decision-making step is required to find each centroid's best ordering, which, for instance, can be obtained by finding the most frequent ordering among the points of the training dataset associated with that centroid (majority rule).

$$C_u^* = \text{majority} \{C_r^*\}_{r:u_r \in u}, \text{ for } u = 1, \dots, K_c.$$

The summary of the suggested clustering algorithm is provided in the form of pseudocode under **Algorithm 1**. To analyze its performance with respect to the number of the centroids \$K_c\$, we define the distortion (or cost function) \$A(R)\$ as follows:²

$$A(R) = \frac{1}{R} \sum_{r=1}^R \|\mathbf{e}_r - \mathbf{q}_{u_r}\|_1. \quad (8)$$

In Fig. 4, the distortion function \$A(R)\$ is calculated using a simulation-based dataset with \$R = 4000\$ elements, and an average SNR per subcarrier \$\bar{\rho}_l = 10\$ dB for all vehicles. Notice that as the value of \$K_c\$ increases, the number of dataset points per cluster decreases, which may improve not only the accuracy of clustering, but also the convergence speed. On the contrary, a small number of clusters can lead to ambiguity due to the long distance separation between each centroid and the cluster edge members. Therefore, the effectiveness of clustering can be enhanced by properly finding the elbow point of \$K_c\$. In Fig. 4, the distortion curves for all selection rules monotonically decrease as the value of \$K_c\$ increases, and they have elbow points around \$K_c = 50\$ clusters. This means that increasing the number of clusters beyond \$K_c = 50\$ reduces the intra-cluster distances only by little. In this light, we can argue that \$K_c = 50\$ is a good choice for the given dataset, as

²Since the variations of \$\mathbf{e}_r\$ under fading are random variables, the mean squared deviation error function of the K-Means clustering can take high values due to the long distances of the cluster edge members within each cluster. Therefore, for this learning model, we consider the mean absolute deviation error function also known as the 1-norm error.

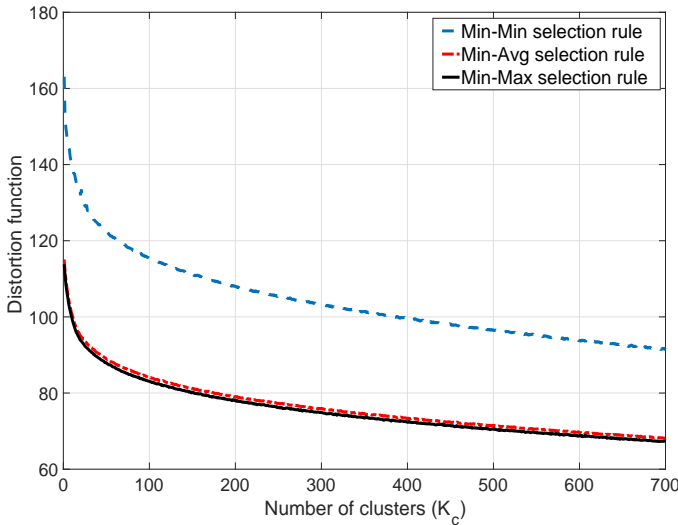


Fig. 4: Comparison of the distortion function with respect to the number of clusters for various selection rules.

it strikes a good balance between accuracy and computational complexity.

D. Mini-batch K-Means learning algorithm

As the size of the dataset increases, the computation time of K-Means clustering increases too, and more importantly, the algorithm convergence requires an increasing number of iterations, which can quickly make the algorithm implementation impractical. To efficiently handle a large dataset, we consider the mini-batch K-Means method for off-line training [27]–[29]. According to it, we break the dataset into smaller randomly grouped batches of size b_s . Given the size R of the dataset, the BS randomly divides the dataset into b_n batches such that $b_n = \lfloor \frac{R}{b_s} \rfloor$. Afterward, the BS applies the training process described under **Algorithm 1** to the individual batches. The updated centroids of the first batch are used as initial values for the training in the next batch, and so forth. Finally, the algorithm returns the centroids based on the computed clustering in the last batch. The convergence of the mini-batch K-Means can be faster than a single batch K-Means clustering because it can reduce the required number of iterations by jointly tuning the initial centroids across the batches. The performance of the mini-batch K-Means will be illustrated in Section V, taking into consideration the reliability-complexity trade-off during off-line training.

E. Cross-Validation algorithm

In this section, we formulate a cross-validation model to evaluate the effectiveness of the trained clusters. The cross-validation indicates how well the trained model is generalized on unseen data, and can help to select the number of clusters that avoid underfitting or overfitting³ [39].

³In underfitting case, the model cannot predict the training data well. Thus, a validation error in statistics occurs when the model is either the underlying trend of the data members or does not generalize to new data. In overfitting case, the model predicts the training data too well. Thus, a validation error in statistics occurs when a model is too closely aligned to a limited set of data members.

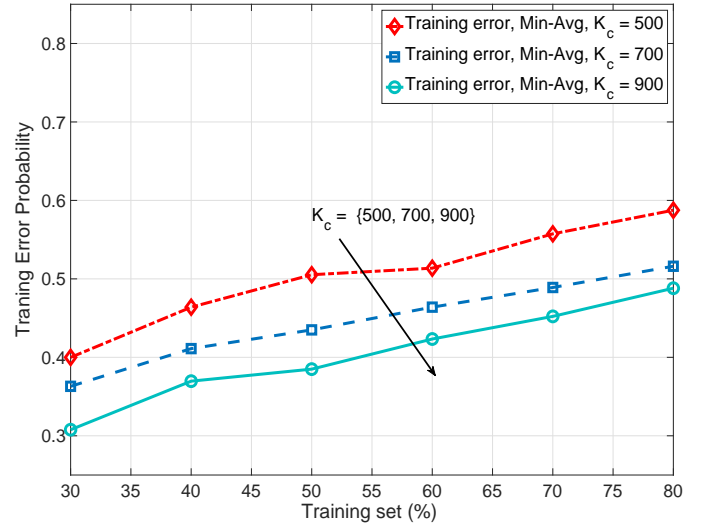


Fig. 5: The impact of the size of the training subset (from 30% to 80%) on the training error for different numbers of clusters (K_c). The simulation-based dataset with size $R = 4000$ is used to evaluate the training error probability.

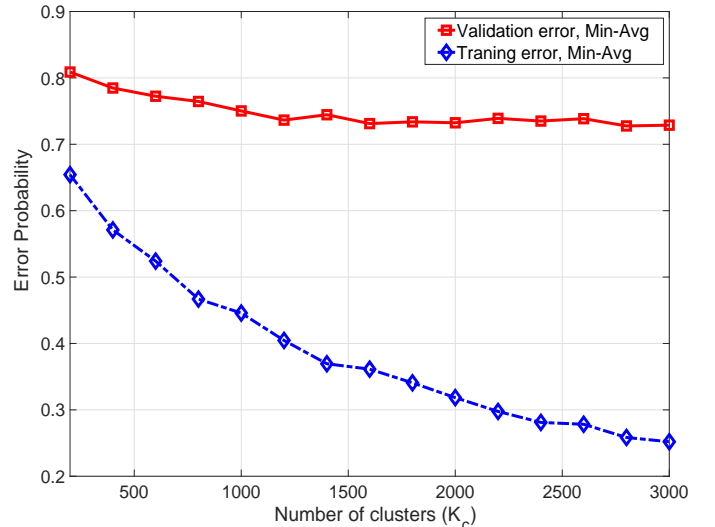


Fig. 6: Validation and training error probabilities with respect to the number of clusters (K_c) when the combined dataset with size $R = 14000$ is used. The training and validation subsets are 70% and 30% of the training dataset, respectively.

1) *Training error probability*: In this approach, the training dataset $\{\tilde{\mathbf{e}}_r\}_{r=1}^R$ is randomly shuffled and then divided into two subsets: the training subset \mathbf{e}_t and the validation subset \mathbf{e}_v , $\{\tilde{\mathbf{e}}_r\}_{r=1}^R = \mathbf{e}_t \cup \mathbf{e}_v$, at a ratio, e.g., 70 : 30 or 80 : 20. The error probability for the training subset can be measured by comparing the best ordering of each centroid (obtained for instance by the majority rule) and the ordering of its members. In Fig. 5, one may see the impact of the size of the training subset onto the training error probability. It is illustrated that the training error probability decreases as the value of K_c increases and/or the size of the training subset decreases. Therefore, in the given training set, we may control the ratio between the training and validation subsets to improve

the training error performance.

2) *Validation and the number of clusters*: The clusters and the centroids are first learned on the training subset \mathbf{e}_t and then their accuracy is assessed on the validation subset \mathbf{e}_v . We can measure the number of erroneous orderings in the validation subset and calculate the error probability. Fig. 6 depicts the error probability during validation with respect to the number of clusters for a combined dataset of size $R = 14000$ and average SNR per subcarrier $\bar{\rho}_l = 10$ dB for all vehicles. The training error probability decreases with the number of clusters and becomes less than 0.4 at around $K_c = 1500$ clusters. In Fig. 6, we can also observe that as the value of K_c increases, the validation error probability decreases, but it flattens out after $K_c = 1500$, indicating that the selection of approximately 1500 clusters is a reasonable choice. While Fig. 6 illustrates the underfitting for a number of clusters $K_c < 1500$, the case of overfitting is not demonstrated, but since the validation error probability tends to have a convex shape [39], overfitting will appear for a large value of $K_c > 3000$. To improve the validation error probability and fine-tune the centroids, we can repeat the training and validation processes several times selecting different subsets \mathbf{e}_t and \mathbf{e}_v each time.

Based on the behavior of the validation and training error probabilities, we can find the number of clusters K_c^* within an acceptable value (threshold) of the training error. If this is not possible, we need to reconstitute, e.g., augment the training dataset \mathbf{e}_r . Note that the number of clusters obtained here is a generalized value for the training dataset including unseen data, whereas the one obtained from the distortion function in Fig. 4 is limited to the given training dataset.

F. Theoretical SEP

To reduce the training time, we adopt the principle of transfer learning, see for instance [25], [26], where the cluster centroids can be initialized using closed-form approximations for the SEP, and subsequently fine-tuned with a limited dataset based on simulations. To this end, the derived theoretical expressions for the SEPs will help quickly generate the training dataset. We summarize the SEPs for all the vehicles below and at the top of the next page as equations (9)-(11), while the derivation details can be found in the Appendix. For the vehicle with the worst channel conditions, V_L , recall that IM is used and the SEP can be approximated as $P_L \approx$

$$\frac{1}{12} \exp\left(-\frac{\bar{\rho}_L \|\check{\mathbf{H}}_L\|_F^2}{4}\right) + \frac{1}{4} \exp\left(-\frac{\bar{\rho}_L \|\check{\mathbf{H}}_L\|_F^2}{3}\right). \quad (9)$$

IV. TESTING FOR LEARNING-DRIVEN PIMA

In real-time operation, the BS can use the learning outcomes for ordering the vehicles given the measured $N \times L$ uplink energy observations from L vehicles over N subcarriers. The BS does not anymore need to estimate the downlink CSIs and numerically solve the optimization problem in Eq. (5). Instead, it finds the nearest cluster to the measured vector of uplink energies and estimates an effective ordering of vehicles from

the selected cluster's centroid. The user ordering in real-time operation is therefore selected as follows:

$$C^* = C_u^* : \arg \min_u \|\mathbf{q}_u - \hat{\mathbf{e}}\|, \text{ for } u = 1, \dots, K_c, \quad (12)$$

where $\hat{\mathbf{e}}$ is the measured energy vector during testing.

Therefore the time complexity of user ordering during testing is $\mathcal{O}(K_c)$. Given the selected ordering of vehicles, the BS can quickly generate PIMA signals in the downlink as shown in Fig. 7 without estimating the full CSIs, i.e., amplitude and phase, across the vehicles and subcarriers. Similarly, the trained cluster set can be used to estimate effective vehicle orderings for all blocks G spanning over the N_t subcarriers.

V. EVALUATION RESULTS

In this section, we use simulations to evaluate the symbol error probability (SEP) performance of the proposed learning-driven PIMA scheme, and compare it with benchmarking algorithms. A key takeaway point from this section is that the K-Means clustering algorithm for ordering the vehicles in PIMA generalizes well to unseen SNRs during training, which mitigates the requirement for generating large training datasets. Furthermore, we show that the closed-form mathematical approximations for the SEP of PIMA derived in Section III-F can be effectively used for transfer learning.

A. Parameter settings

To generate a realistic simulation setup, we adopt the parameter settings of Long-Term Evolution (LTE) for the speed of vehicles and the subcarrier spacing, i.e., the speed per vehicle is randomly generated in the interval 50 – 200 km/h and the subcarrier spacing is set at 15 kHz. It is straightforward to adapt the parameter values to the Fifth Generation New Radio (5G NR) or Cellular Vehicle-to-Everything (C-V2X) communication scenarios.

We consider $L = 4$ vehicles⁴, $M = 4$, i.e., Quadrature Phase Shift Keying (QPSK) constellation for superposition modulation unless otherwise stated, $N = 4$ subcarriers and $k = 2$ active subcarriers for index modulation (IM). For the superposed signals, we set the power allocation ratio $a_l^2/a_1^2 = 10$ dB for $l \in \{2, 3\}$. Recall that repetition coding over the active subcarriers is employed for the vehicle V_1 and IM is used for $V_4 (= V_L)$. Note that V_1 and V_4 are always the vehicles with the best and the worst propagation channel conditions, respectively, in every TTI. For clarity, we do not consider power control in the uplink.

For $L = 4$ vehicles and $N = 4$ subcarriers, the energy vector \mathbf{e}_r in the training dataset has dimensions 16×1 . To identify an effective ordering of vehicles C_r^* for a given selection rule and create the training dataset $\tilde{\mathbf{e}}_r = \{\mathbf{e}_r, C_r^*\}$,

⁴Notice that in NOMA, as the number of multiplexed users increases, the capacity gain of NOMA increases too. However, NOMA is more efficient for a small number of users due to interference constraints and error propagation [40]. In fact, multi-user superposed transmission (MUST) was introduced in 3rd Generation Partnership Project (3GPP) Release 13 to enable NOMA for a small number of users. In particular, MUST was proposed to realize downlink multi-user superposition transmission in LTE-Advanced systems, focusing on the multiplexing of two users only. Therefore, in this simulation, we use $L = 4$ vehicles, where the multiplexing of two vehicles per active subcarrier is considered.

$$P_1 \approx \left[\frac{M-1}{M} - \left[\frac{1}{6} \exp(-2\tau_1) + \frac{1}{2} \exp\left(-\frac{8}{3}\tau_1\right) \right] \right] \left[\frac{1}{12} \exp\left(-\frac{\bar{\rho}_1 \|\check{\mathbf{H}}_1\|_F^2}{4}\right) + \frac{1}{4} \exp\left(-\frac{\bar{\rho}_1 \|\check{\mathbf{H}}_1\|_F^2}{3}\right) \right] + \left[\frac{1}{6} \exp(-2\tau_1) + \frac{1}{2} \exp\left(-\frac{8}{3}\tau_1\right) \right], \text{ where } \tau_1 = \beta_M \bar{\rho}_1 a_1^2 \sum_{\nu=1}^2 z_{1i_\nu}. \quad (10)$$

$$P_l \approx \left[\frac{M-1}{M} - \left[\frac{1}{6} \exp(-\tau_2) + \frac{1}{2} \exp\left(-\frac{4}{3}\tau_2\right) \right] \right] \left[\frac{1}{12} \exp\left(-\frac{\bar{\rho}_l \|\check{\mathbf{H}}_l\|_F^2}{4}\right) + \frac{1}{4} \exp\left(-\frac{\bar{\rho}_l \|\check{\mathbf{H}}_l\|_F^2}{3}\right) \right] + \left[\frac{1}{6} \exp(-\tau_2) + \frac{1}{2} \exp\left(-\frac{4}{3}\tau_2\right) \right], \text{ where } \tau_2 = \frac{\beta_M 2 \bar{\rho}_l a_l^2 z_{li_\nu}}{2 \bar{\rho}_l a_l^2 z_{li_\nu} + 1}. \quad (11)$$

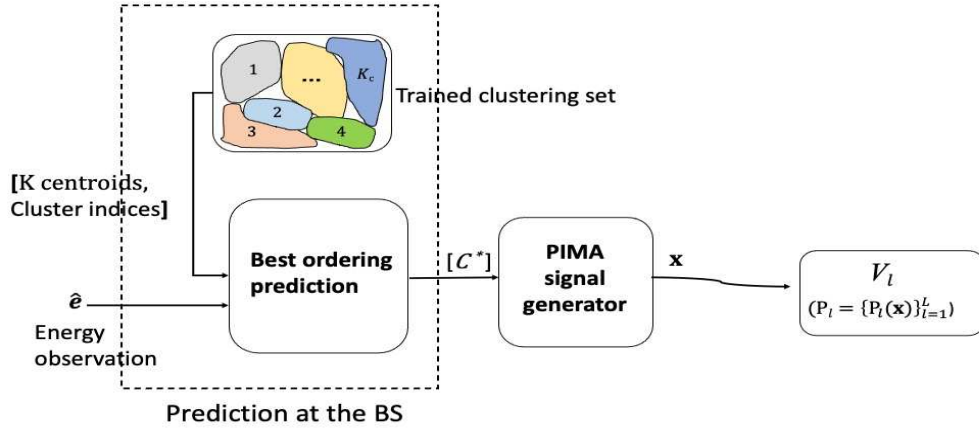


Fig. 7: Learning-driven PIMA in real-time.

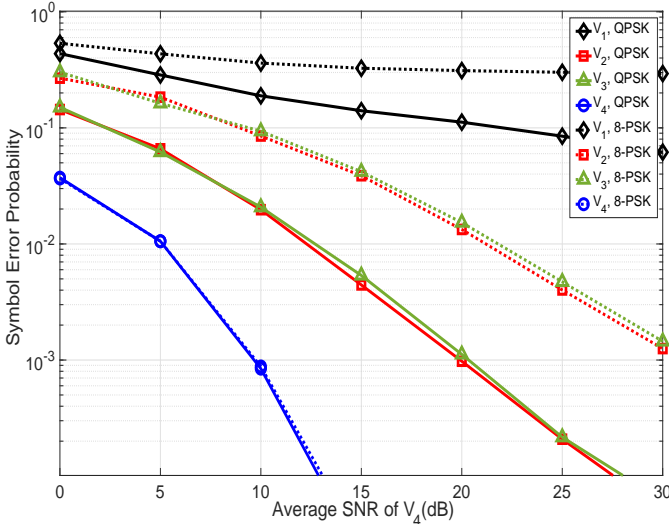


Fig. 8: The SEP of the proposed learning-driven PIMA for each vehicle using the Min-Avg selection rule. For the vehicles $V_l, l \in \{1, 2, 3\}$ two different modulation schemes are considered, i.e., $M = 4$ (QPSK) and $M = 8$ (8-PSK).

we also use the mathematical approximations for the SEP derived in Section III-D (transfer learning). The simulation-based

training dataset is denoted by $\{\tilde{\mathbf{e}}_r\}_{r=1}^{R_1}$, where $R_1 = 4000$ and the theory-based training dataset is denoted by $\{\tilde{\mathbf{e}}_r\}_{r=R_1+1}^{R_1+R_2}$, where $R_2 = 10000$, yielding a combined dataset of size $R = R_1 + R_2 = 14000$ elements. The training datasets are generated by performing 100000 simulations at an average SNR per subcarrier $\bar{\rho}_l = 10$ dB for all vehicles. For K-means clustering, we utilize $K_c^* = 1500$ clusters, which is obtained in Section III-E, unless otherwise stated.

B. Discussion of the results

Fig. 8 depicts the SEP of the proposed learning-driven PIMA when the channel ratio is $\bar{\rho}_l/\bar{\rho}_4 = 5$ dB for the vehicles $V_l, l \in \{1, 2, 3\}$. The vehicle under the worst instantaneous channel condition (V_4) outperforms all other vehicles as it uses IM. In particular, it obtains $\text{SEP} = 10^{-3}$ at SNR 12 dB while the other vehicles obtain the same SEP at SNR around 25 dB. Interestingly, the SEP curves for the vehicles with the best (V_1) and mild channel conditions (V_2, V_3) follow similar trends. The SEP of V_1 is constantly higher than that of V_2 and V_3 , but their gap eventually gets smaller at high SNRs, as V_1 benefits from repetition coding. As expected, the SEP of $V_l, l \in \{1, 2, 3\}$ increases for increasing modulation order.

Fig. 9 illustrates the system's SEP calculated as being equal to the average SEP of the vehicles and compares the learning-driven PIMA with benchmarking algorithms for user ordering

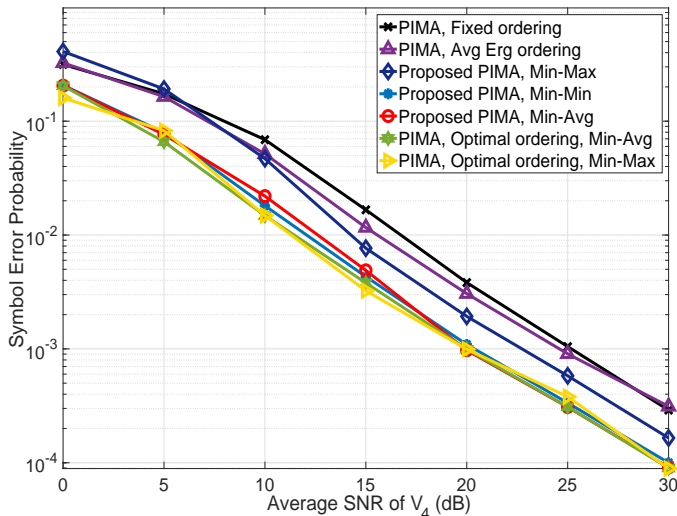


Fig. 9: Comparison of the system's SEP for the proposed learning-driven PIMA with three selection rules, and PIMA with average energy-based ordering, and fixed ordering. **The system's SEP with optimal ordering obtained using exhaustive search during real-time inference is also depicted for every selection rule.**

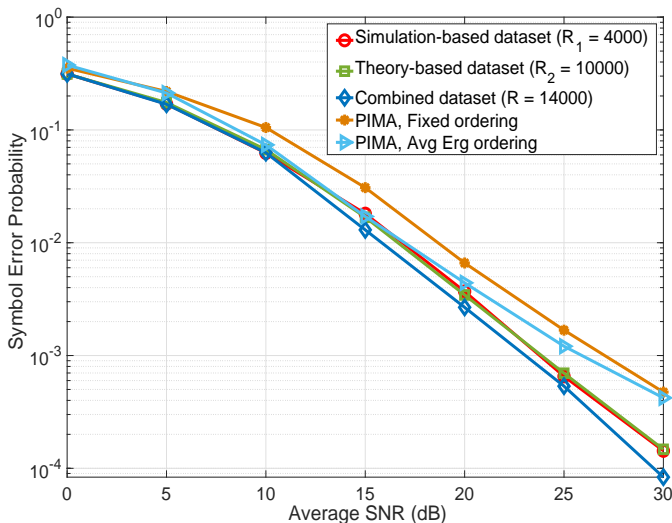


Fig. 10: The system SEP, calculated as the average SEP over the four vehicles, of the learning-driven PIMA with different training datasets, i.e., simulation-based, theory-based and combined dataset is depicted. **For benchmarking purposes, the system SEP is also depicted for fixed-based ordering as well as ordering based on the average received energies across the subcarriers.**

when the channel ratio is $\bar{\rho}_l/\bar{\rho}_4 = 5$ dB for the vehicles $V_l, l \in \{1, 2, 3\}$. The PIMA schemes using average energy-based ordering (the average of all energies over $N = 4$ subcarriers of each vehicle), and fixed ordering are selected for benchmarking. The SEPs based on Min-Avg and Min-Min selection rules attain the best performance and clearly outperform the benchmarks, while obtaining approximately 5 dB power gain at $\text{SEP} \leq 10^{-3}$ over the energy-based

or fixed-based order counterparts. It becomes also evident from Fig. 9 that the learning-driven PIMA generalizes well to different average SNRs than that used for training (10 dB). **The accuracy of the training algorithm is also demonstrated in Fig. 9. One can see over there that using exhaustive search during real-time inference too, only gives a marginal improvement in the SEP for the Min-Avg and the Min-Min selection rules.**

Fig. 10 depicts the system's SEP using different training datasets, i.e., simulation-based $\{\tilde{\epsilon}_r\}_{r=1}^{R_1}$, theory-based $\{\tilde{\epsilon}_r\}_{r=R_1+1}^R$, and combined $\{\tilde{\epsilon}_r\}_{r=1}^R$. We can see over there that the simulation-based dataset performs close to the theory-based dataset. This observation validates the accuracy of the approximations for the SEPs developed in Section III-F. At the same time, generating the theory-based dataset consumes much less computational resource than that needed to generate the simulation-based dataset. The combined dataset benefits from both simulation-based and theory-based datasets leading to a marginal improvement in the performance.

Next, we study the performance-complexity trade-off during training by simulating the mini-batch K-means algorithm. Fig. 11 shows the SEP of the learning-driven PIMA using the mini-batch K-Means clustering with different number of mini-batches, $b_n \in \{1, 2, 3, 4\}$, and their associated distortion curves at an average SNR per subcarrier $\bar{\rho}_l = 10$ dB for all vehicles. As expected, the system SEP using four mini-batches obtains the worst SEP performance, at the fastest training convergence [39]. Note that during simulations, e.g., using Matlab, the K-Means clustering with a large dataset may face convergence problems even after several iterations (e.g., 100 iterations). Interestingly, the simulations have showed that the centroids using more than one mini-batch can successfully converge in less than 100 iterations when $R = 14000$. To sum up, using four mini-batches strikes a good balance between performance and complexity as the SEP for two and four mini-batches is practically the same, but considering only one batch, vehicles can achieve the highest reliability, which is important for safety-related functions.

C. Simulation with synthetic mobility traces of vehicles

Next, we simulate the performance of the learning-driven PIMA with synthetic traces for the locations of vehicles along multi-lane highways [30], [31], as shown in Fig. 12. For this, the mean received signal power level per subcarrier and vehicle in the uplink is computed as $\omega_l^{-\psi}$, where ω_l is the distance between the vehicle V_l and the BS, and the path-loss exponent is $\psi = 3$ [41]. We consider a cell with radius 1 km, where the coordinates (x, y) of each vehicle change in $0 \leq x \leq 2000$ m, and $y \in \{3, 6, 9\}$ m as it travels within the cell. The BS is located at the roadside in the middle of the cell, i.e., $(x_{BS}, y_{BS}) \equiv (1000, 0)$. For generating the training dataset, we randomly select four vehicles within the cell and generate their channel matrices for small scale fading $\mathbf{H}_l = \text{diag}(h_{l1}, \dots, h_{lN})$, where the element h_{ln} follows the complex-valued Gaussian distribution with zero mean and unit variance, i.e., $h_{ln} \sim \mathcal{CN}(0, 1)$. The complex Gaussian distributions are independently sampled every 10 ms till one

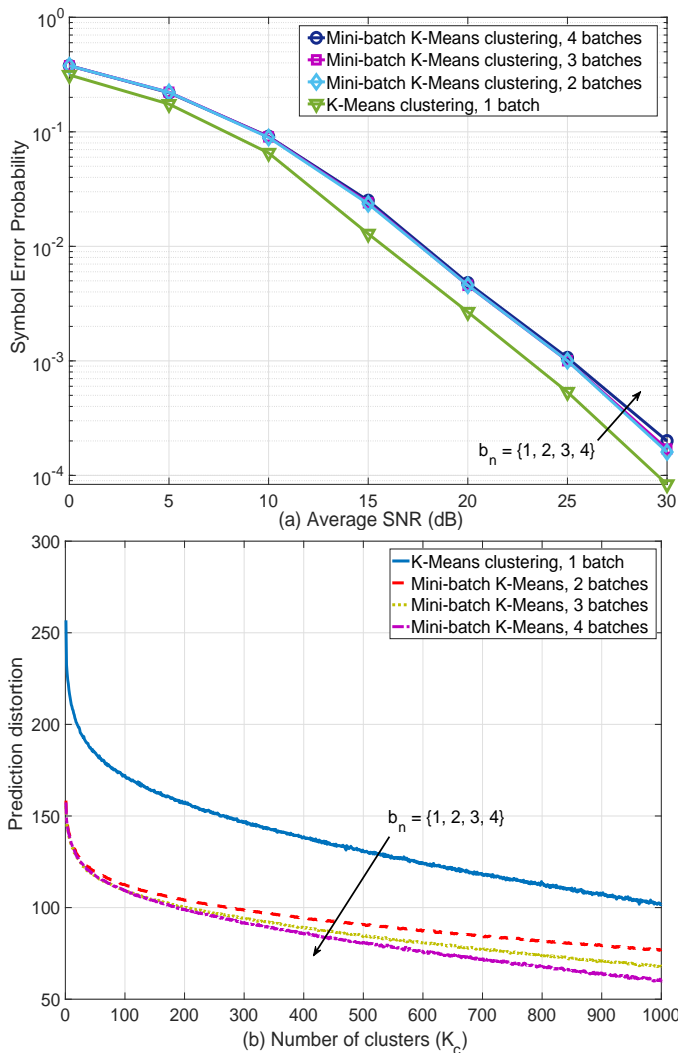


Fig. 11: Comparisons of the system SEP calculated as the average SEP over the four vehicles (a) and the distortion function when $\bar{\rho}_l = 10$ dB for all vehicles (b) for the Mini-batch K-Means clustering with different numbers of batches.

of the vehicles crosses the cell boundary. For simplicity, no Doppler spread is considered in that case. Then, we repeat the same procedure for four other vehicles till the training dataset is constructed. For K-Means clustering, we consider a combined training dataset $R = 30,000$ ($R_1 = 4000$ using simulations, and $R_2 = 26,000$ using the approximations for the SEP obtained in Section III-D) and $K_c = 3000$ clusters because the size of the dataset is now larger.

During testing, we have simulated 10^5 PIMA signal transmissions and counted that the ordering of vehicles has changed with probability about 70 % between consecutive transmissions, i.e., every 10 ms. This observation validates the effectiveness of the learning-driven PIMA in a dynamically changing V2X scenario.

Fig. 13 illustrates the comparison between the SEP of the learning-driven PIMA and the two benchmarks, i.e., distance-based and fixed ordering. The learning-driven PIMA outperforms the benchmarking schemes in terms of maximum,

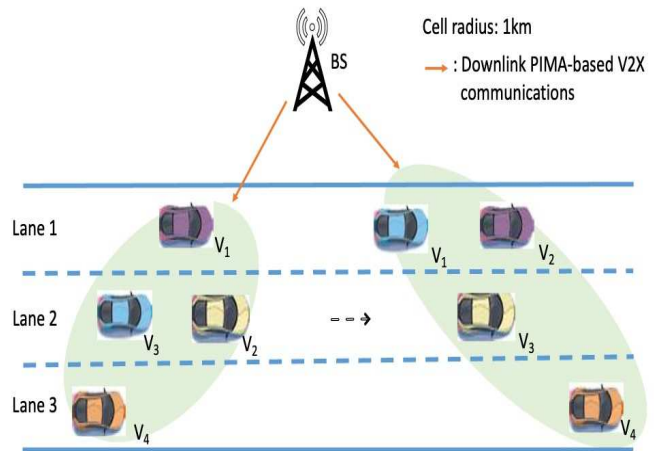


Fig. 12: System model illustration of a V2X system with synthetic data traces for the locations of vehicles along multi-lane highways. The vehicles within the same group experience different average SNRs and their ordering may change with time due to mobility.

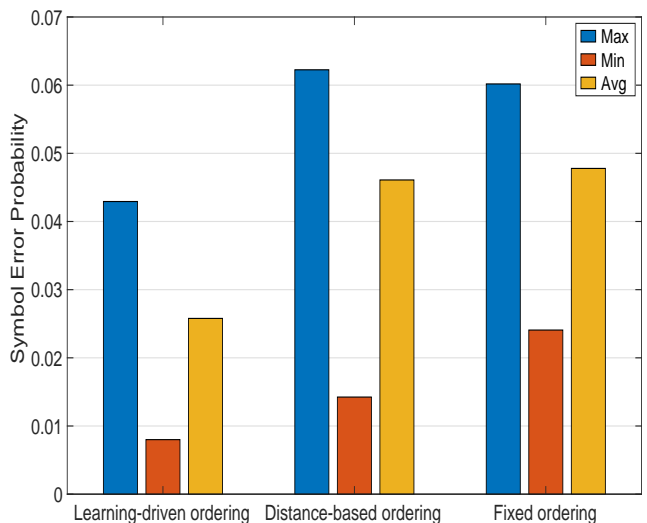


Fig. 13: Comparisons of system's SEP of the proposed learning-driven PIMA with distance-based and fixed ordering using the synthetic data traces for the locations of vehicles.

minimum and average SEP. This observation validates that the learning-driven PIMA is beneficial with realistic motorway traffic too. Note that the performance difference between learning-driven and distance-based ordering is due to the impact of fast fading onto the user ordering, which can be captured only by the learning-driven scheme.

VI. CONCLUSIONS

The study in this paper revealed that the use of a bespoke unsupervised K-Means clustering model for identifying an effective user ordering in PIMA outperformed the existing baseline schemes (based on average energy-based and fixed orderings). We obtained a promising 5 dB power gain at SEP =

10^{-3} without increasing much the implementation complexity of the ordering algorithm. The proposed scheme does not require the estimation of CSIs, as it uses the received energies across the users and subcarriers in the uplink to effectively order the users. It is also shown that the Min-Avg and Min-Min selection rules outperformed the Min-Max rule, yielding 2.5 dB power gains at $\text{SEP} = 10^{-3}$. Following the principle of transfer learning, we derived generalized theoretical approximations for the SEPs, which were used to generate part of the training dataset and subsequently reduce the computational complexity during offline training. Furthermore, in realistic motorway mobility traces, the PIMA scheme using learning-driven ordering showed better SEP (50% reduction) than distance-based ordering. We hope that the promising results of this paper can motivate further research in model-aided machine learning approaches for multiple access in next generation vehicular networks and similar applications.

APPENDIX

DERIVATION OF SYMBOL ERROR PROBABILITIES (SEPs)

We formulate a theoretical model for the SEP of PIMA for each vehicle $V_l, l = 1, \dots, L$ to help quickly generate the training dataset in Section III-F. In order to obtain the SEP from equation (2), each vehicle uses maximum likelihood (ML) detection [10], [11], which can be read as

$$\hat{\mathbf{x}}_l = \arg \min_{\mathbf{x}} \|\mathbf{y}_l - \sqrt{\bar{\rho}_l} \check{\mathbf{H}}_l \mathbf{x}\|^2, 1 \leq l \leq L. \quad (\text{A.1})$$

A. Symbol error probability of V_L

Once $\hat{\mathbf{x}}_L$ in equation (A.1) is obtained, the IM symbol $\hat{x}_{\mathcal{I}}$ is estimated using a Table similar to Table II. In order to generate a mathematical expression for the SEP of V_L , P_L , we start with the index error probability (IEP), denoted by $P(\alpha \rightarrow \tilde{\alpha})$, which describes the probability that the transmitted IM symbol \mathcal{I}_α is incorrectly estimated as $\mathcal{I}_{\tilde{\alpha}}$, where $\alpha, \tilde{\alpha} \in \{1, \dots, N_{\mathcal{I}}\}$, $\alpha \neq \tilde{\alpha}$ and $N_{\mathcal{I}}$ is the number of IM symbols. Thus, using a union bound for given α , N and k , and referring to the well-known Pairwise Error Probability (PEP) in [42], the conditional IEP of the symbol $x_{\mathcal{I}}$ at V_L can be provided by

$$P_{IL}(\alpha) \leq \sum_{\tilde{\alpha}=1, \tilde{\alpha} \neq \alpha}^{N_{\mathcal{I}}-1} P(\alpha \rightarrow \tilde{\alpha}) = \sum_{\tilde{\alpha}=1, \tilde{\alpha} \neq \alpha}^{N_{\mathcal{I}}-1} Q\left(\sqrt{\frac{d_L^2}{4}}\right), \quad (\text{A.2})$$

where $d_L^2 = \bar{\rho}_L \|\check{\mathbf{H}}_L \mathbf{x} - \check{\mathbf{H}}_L \tilde{\mathbf{x}}\|^2$ is the squared Euclidean distance between PIMA signals associated to \mathcal{I}_α and $\mathcal{I}_{\tilde{\alpha}}$, and $Q(x) := \pi^{-1} \int_0^{\pi/2} e^{-x^2/2 \sin^2 \theta} d\theta$ is the error function.

Using the law of total probability and equation (A.2), the SEP at V_L can be upper bounded as

$$P_L = \frac{k}{N} \sum_{\alpha=1}^{N_{\mathcal{I}}} P_{IL}(\alpha) \leq \frac{k}{N} \sum_{\alpha=1}^{N_{\mathcal{I}}} \sum_{\tilde{\alpha}=1, \tilde{\alpha} \neq \alpha}^{N_{\mathcal{I}}-1} Q\left(\sqrt{\frac{d_L^2}{4}}\right). \quad (\text{A.3})$$

Based on the structure of PIMA signals, notice that we can reduce $d_L^2 \approx \bar{\rho}_L \|\check{\mathbf{H}}_L\|_F^2 P_t N/k = 2\bar{\rho}_L \|\check{\mathbf{H}}_L\|_F^2$. Also, P_{IL} can be simplified to a single Q -function term due to the orthogonality of index combinations. After simple manipulations using the tight approximation of the Q -function,

i.e., $Q(x) \approx 1/12 \exp(-x^2/2) + 1/4 \exp(-2x^2/3)$, and equation (A.3), the approximate SEP of V_L can be obtained as equation (9) in Section III-F.

B. Symbol error probability of V_1

The vehicle V_1 first detects $\hat{x}_{\mathcal{I}}$ and then employs SIC in order to detect s_1 . To do that, V_1 detects and removes all signals $s_l, l = 2, \dots, L-1$ from each of the k active subcarriers. In this work, we consider perfect SIC for presentation clarity. After SIC, equation (2) reduces to:

$$\mathbf{y}_1 = \sqrt{\bar{\rho}_1} \check{\mathbf{H}}_1 \mathbf{x}_1 + \mathbf{n}_1. \quad (\text{A.4})$$

Employing the ML detection independently on the k active subcarriers allows to detect s_1 . The resulting instantaneous SNR of the active subcarriers $i_\nu, \nu = 1, \dots, k$ is

$$\rho_{1i_\nu} = \bar{\rho}_1 \frac{a_1^2 P_t N}{k} |\theta_{i_\nu f} h_{1i_\nu}|^2 = \bar{\rho}_1 2a_1^2 |\theta_{i_\nu f, 1} h_{1i_\nu}|^2. \quad (\text{A.5})$$

Due to the repetition coding of symbol s_1 onto $k = 2$ active subcarriers, applying the maximal ratio combining can produce the effective instantaneous SNR of V_1 as

$$\rho_1 = 2\bar{\rho}_1 a_1^2 \sum_{\nu=1}^2 |\theta_{i_\nu f, 1} h_{1i_\nu}|^2. \quad (\text{A.6})$$

Notice that V_1 intends to detect s_1 from k active subcarriers, whose indices need to be first obtained from the detection of the IM symbol of V_L . Thus, the symbol error event (e_1) at V_1 may occur under the following two conditions: Correct detection of $x_{\mathcal{I}}$ ($\hat{x}_{\mathcal{I}} = x_{\mathcal{I}}$); and incorrect detection of $x_{\mathcal{I}}$ ($\hat{x}_{\mathcal{I}} \neq x_{\mathcal{I}}$). Accordingly, the SEP at V_1 consists of two terms:

$$\begin{aligned} P_1 &= P(e_1, x_{\mathcal{I}} \neq \hat{x}_{\mathcal{I}}) + P(e_1, x_{\mathcal{I}} = \hat{x}_{\mathcal{I}}) \\ &= \frac{M-1}{M} P_{I1} + P_{C1}(\rho_1)(1 - P_{I1}), \end{aligned} \quad (\text{A.7})$$

where $M = |S|$ is the constellation size for the vehicles $V_l, l = 1, \dots, L-1$, P_{I1} denotes the overall IEP of $x_{\mathcal{I}}$ at V_1 , the ratio $(M-1)/M$ represents the conditional error probability for s_1 for $\hat{x}_{\mathcal{I}} \neq x_{\mathcal{I}}$, and $P_{C1}(\cdot)$ is the error probability of M -ary complex symbols, i.e., $P_{C1}(\rho_1) \approx 2Q(\sqrt{2\rho_1} \sin(\pi/M))$ for M -ary Phase Shift Keying (MPSK) for $M > 2$ [43, Eq. 5.2.61].

Notice that P_{I1} in equation (A.7) can be obtained by similar steps used to obtain P_L , and equation (A.7) can be finally rewritten as

$$P_1 = \left(\frac{M-1}{M} - P_{C1}(\rho_1)\right) P_{I1} + P_{C1}(\rho_1), \quad (\text{A.8})$$

where P_{I1} is

$$P_{I1} \leq \frac{k}{N} \sum_{\alpha=1} \sum_{\tilde{\alpha} \neq \alpha} Q\left(\sqrt{\frac{\bar{\rho}_1 \|\check{\mathbf{H}}_1\|_F^2}{2}}\right). \quad (\text{A.9})$$

After substituting the approximation for the Q -function in the expression of $P_{C1}(\rho_1)$ we get

$$\begin{aligned} P_{C1}(\rho_1) &\approx \frac{1}{6} \exp\left(-2\beta_M \bar{\rho}_1 a_1^2 \sum_{\nu=1}^k z_{1i_\nu}\right) \\ &+ \frac{1}{2} \exp\left(-\frac{8}{3}\beta_M \bar{\rho}_1 a_1^2 \sum_{\nu=1}^k z_{1i_\nu}\right), \end{aligned} \quad (\text{A.10})$$

where $\beta_M = \sin^2(\pi/M)$ is the M -ary constellation dependent constant, and $z_{l_{i_v}} = |\theta_{i_v f, l} h_{l_{i_v}}|^2$.

Finally, after substituting equations (A.9) and (A.10) into equation (A.8), the SEP of V_l can be derived as equation (10) shown in Section III-F.

C. Symbol error probability of $V_l, l = 2, \dots, L-1$

After estimating \hat{x}_l and subsequently the IM symbol $\hat{x}_{\mathcal{I}} = \{\hat{i}_1, \hat{i}_2\}$, the vehicle V_l can detect s_l . Firstly, V_l needs to employ SIC to subtract all s_j for $l < j < L$. Then, V_l detects s_l , treating s_1 and s_j for $1 < j < l$ as noises. Therefore, the corresponding SINR at V_l is given by

$$\rho_l = \frac{2\bar{\rho}_l a_l^2 P_t |\theta_{i_v f, l} h_{l_{i_v}}|^2}{2\bar{\rho}_l a_l^2 P_t |\theta_{i_v f, l} h_{l_{i_v}}|^2 + 1}, \quad (\text{A.11})$$

where $a_l^2 = a_1^2 + \sum_{j \in l_e}^{l-1} a_j^2$ for $l \in l_e$ and $a_l^2 = a_1^2 + \sum_{j \in l_o}^{l-1} a_j^2$ for $l \in l_o$.

Accordingly, the SEP can be determined by the conditional estimation of s_l under the IM symbol detection at V_l , which is similar to the steps used in V_1 . Thus, the SEP of V_l can be expressed in two parts and is approximated in the following

$$P_l = P(e_l, \hat{x}_{\mathcal{I}} \neq x_{\mathcal{I}}) + P(e_l, \hat{x}_{\mathcal{I}} = x_{\mathcal{I}}), \quad (\text{A.12})$$

where e_l is the error event at vehicle V_l .

Referring to ρ_l in equation (A.11), the error probability of M -ary complex symbols at V_l can be obtained in closed-form, with respect to the SINR: $P_{Cl} \approx$

$$\frac{1}{6} \exp\left(-\frac{2\beta_M \bar{\rho}_l a_l^2 z_{l_{i_v}}}{2\bar{\rho}_l a_l^2 z_{l_{i_v}} + 1}\right) + \frac{1}{2} \exp\left(-\frac{4}{3} \frac{2\beta_M \bar{\rho}_l a_l^2 z_{l_{i_v}}}{2\bar{\rho}_l a_l^2 z_{l_{i_v}} + 1}\right), \quad (\text{A.13})$$

where $z_{l_{i_v}} = |\theta_{i_v f, l} h_{l_{i_v}}|^2$.

Using equation (A.13) and a closed-form approximation of error probability of V_l 's IM symbol, the approximate SEP of V_l can be derived as equation (11) shown in Section III-F.

REFERENCES

- [1] B. Di, L. Song, Y. Li, and G. Y. Li, "Non-orthogonal multiple access for high-reliable and low-latency V2X communications in 5G systems," *IEEE J. Sel. Areas Commun.*, vol. 35, no. 10, pp. 2383–2397, Oct. 2017.
- [2] G. Liu, Z. Wang, J. Hu, Z. Ding, and P. Fan, "Cooperative NOMA broadcasting/multicasting for low-latency and high-reliability 5G cellular V2X communications," *IEEE Internet of Things J.*, vol. 6, no. 5, pp. 7828–7838, Oct. 2019.
- [3] D. Zhang, Y. Liu, L. Dai, A. K. Bashir, A. Nallanathan, and B. Shim, "Performance analysis of FD-NOMA-based decentralized V2X systems," *IEEE Trans. Commun.*, vol. 67, no. 7, pp. 5024–5036, Jul. 2019.
- [4] Y. Chen, L. Wang, Y. Ai, B. Jiao, and L. Hanzo, "Performance analysis of NOMA-SM in vehicle-to-vehicle massive MIMO channels," *IEEE J. Sel. Areas Commun.*, vol. 35, no. 12, pp. 2653–2666, Dec. 2017.
- [5] J. Choi, "Non-orthogonal multiple access in downlink coordinated two-point systems," *IEEE Commun. Lett.*, pp. 313–316, Feb. 2014.
- [6] Z. Ding, X. Lei, G. K. Karagiannidis, R. Schober, J. Yuan, and V. K. Bhargava, "A survey on non-orthogonal multiple access for 5G networks: Research challenges and future trends," *IEEE J. Select. Areas Commun.*, vol. 35, no. 10, pp. 2181–2195, Oct. 2017.
- [7] S. M. R. Islam, N. Avazov, O. A. Dobre, and K. S. Kwak, "Power-domain non-orthogonal multiple access (NOMA) in 5G systems: Potentials and challenges," *IEEE Commun. Surveys Tuts.*, vol. 19, no. 2, pp. 721–742, 2nd Quart. 2017.
- [8] S. Lee, T. Q. Duong, and R. Woods, "Impact of wireless backhaul unreliability and imperfect channel estimation on opportunistic NOMA," *IEEE Trans. Veh. Technol.*, vol. 68, no. 11, pp. 10822–10833, Nov. 2019.
- [9] E. Basar, "Index modulation techniques for 5G wireless networks," *IEEE Commun. Mag.*, vol. 54, no. 7, pp. 168–175, 2016.
- [10] E. Basar, U. Aygolu, E. Panayirci, and H. V. Poor, "Orthogonal frequency division multiplexing with index modulation," *IEEE Trans. Signal Processing*, vol. 61, no. 22, pp. 5536–5549, Nov. 2013.
- [11] T. Van Luong and Y. Ko, "Impact of CSI uncertainty on MCIC-OFDM: Tight closed-form symbol error probability analysis," *IEEE Trans. Veh. Technol.*, vol. 67, no. 2, pp. 1272–1279, Feb. 2018.
- [12] Q. Li, M. Wen, E. Basar, H. V. Poor, and F. Chen, "Spatial modulation-aided cooperative NOMA: Performance analysis and comparative study," *IEEE J. Sel. Topics in Signal Process.*, vol. 13, no. 3, pp. 715–728, Jun. 2019.
- [13] X. Chen, M. Wen, T. Mao, and S. Dang, "Spectrum resource allocation based on cooperative NOMA with index modulation," *IEEE Trans. on Cognitive Commun. and Netw.*, vol. 6, pp. 946–958, Sep. 2020.
- [14] A. Tusha, S. Doğan, and H. Arslan, "A hybrid downlink NOMA with OFDM and OFDM-IM for beyond 5G wireless networks," *IEEE Signal Process. Lett.*, vol. 27, pp. 491–495, Mar. 2020.
- [15] E. Arslan, A. T. Dogukan, and E. Basar, "Index modulation-based flexible non-orthogonal multiple access," *IEEE Wireless Commun. Lett.*, vol. 9, no. 11, pp. 1942–1946, 2020.
- [16] S. Lee, M. Dianati, Y. Ko, and A. Mouzakitis, "Power-and-index based multiple access for V2X networks," in *Proc. IEEE 91st Veh. Technol. Conf. (VTC2020 Spring)*, May 2020, pp. 1–6.
- [17] P. Yang, Y. Xiao, Y. L. Guan, M. Di Renzo, S. Li, and L. Hanzo, "Multidomain index modulation for vehicular and railway communications: A survey of novel techniques," *IEEE Veh. Technol. Mag.*, vol. 13, no. 3, pp. 124–134, Sep. 2018.
- [18] Y. Fu, C. Wang, Y. Yuan, R. Mesleh, E. M. Aggoune, M. M. Alwakeel, and H. Haas, "BER performance of spatial modulation systems under 3-D V2V MIMO channel models," *IEEE Trans. Veh. Technol.*, vol. 65, no. 7, pp. 5725–5730, Jul. 2016.
- [19] J. Choi, "On HARQ-IR for downlink NOMA systems," *IEEE Trans. Commun.*, vol. 64, no. 8, pp. 3576–3584, 2016.
- [20] Z. Shi, S. Ma, H. ElSawy, G. Yang, and M.-S. Alouini, "Cooperative HARQ-assisted NOMA scheme in large-scale D2D networks," *IEEE Trans. Commun.*, vol. 66, no. 9, pp. 4286–4302, 2018.
- [21] H. Tabassum, E. Hossain, and J. Hossain, "Modeling and analysis of uplink non-orthogonal multiple access in large-scale cellular networks using poisson cluster processes," *IEEE Trans. Commun.*, vol. 65, no. 8, pp. 3555–3570, 2017.
- [22] M. Salehi and E. Hossain, "On coverage probability in uplink NOMA with instantaneous signal power-based user ranking," *IEEE Wireless Commun. Lett.*, vol. 8, no. 6, pp. 1683–1687, 2019.
- [23] M. Salehi, H. Tabassum, and E. Hossain, "Accuracy of distance-based ranking of users in the analysis of NOMA systems," *IEEE Trans. Commun.*, vol. 67, no. 7, pp. 5069–5083, 2019.
- [24] L. Guo, S. Cong, C. Su, and Z. Sun, "Coverage analysis of downlink NOMA-enabled dense networks with ISP-based user ordering," *IEEE Commun. Lett.*, vol. 24, no. 11, pp. 2440–2444, 2020.
- [25] A. Zappone, M. Di Renzo, M. Debbah, T. T. Lam, and X. Qian, "Model-aided wireless artificial intelligence: Embedding expert knowledge in deep neural networks for wireless system optimization," *IEEE Veh. Technol. Mag.*, vol. 14, no. 3, pp. 60–69, 2019.
- [26] H. He, S. Jin, C.-K. Wen, F. Gao, G. Y. Li, and Z. Xu, "Model-driven deep learning for physical layer communications," *IEEE Wireless Commun.*, vol. 26, no. 5, pp. 77–83, 2019.
- [27] K. Peng, V. C. M. Leung, and Q. Huang, "Clustering approach based on Mini batch K-means for intrusion detection system over big data," *IEEE Access*, vol. 6, pp. 11897–11906, 2018.
- [28] A. Feizollah, N. B. Anuar, R. Salleh, and F. Amalina, "Comparative study of K-means and mini batch K-means clustering algorithms in android malware detection using network traffic analysis," in *2014 Int. Symp. on Biometrics and Security Technol. (ISBAST)*, 2014, pp. 193–197.
- [29] S. R. Fitriyani and H. Murfi, "The K-means with mini batch algorithm for topics detection on online news," in *2016 4th Int. Conf. on Inf. and Commun. Technol. (ICOICT)*, 2016, pp. 1–5.
- [30] D. N. M. F. M. Gramaglia, O. Trullols-Cruces and M. Caldero, "Vehicular networks on two Madrid highways," in *IEEE Int. Conf. Sensing Commun. Netw.*, 2014, p. 423–431.
- [31] —, "Mobility and connectivity in highway vehicular networks: A case study in Madrid," *Elsevier Comput. Commun.*, vol. 78, p. 28–44, 2016.
- [32] K. Koufos and C. Dettmann, "Moments of interference in vehicular networks with hardcore headway distance," *IEEE Trans. Wireless Commun.*, vol. 17, no. 12, p. 8330–8341, 2018.

- [33] K. Koufos and C. P. Dettmann, "The meta distribution of the SIR in linear motorway VANETs," *IEEE Trans. Commun.*, vol. 67, no. 12, p. 8696–8706, 2019.
- [34] Y. Zhao and S. . Haggman, "Sensitivity to doppler shift and carrier frequency errors in OFDM systems-the consequences and solutions," in *Proceedings of Veh. Technol. Conf. (VTC)*, vol. 3, 1996, pp. 1564–1568.
- [35] K. Sathananthan and C. Tellambura, "Probability of error calculation of OFDM systems with frequency offset," *IEEE Trans. Commun.*, vol. 49, no. 11, pp. 1884–1888, 2001.
- [36] A. Hafeez, K. Molnar, H. Arslan, G. Bottomley, and R. Ramesh, "Adaptive joint detection of cochannel signals for TDMA handsets," *IEEE Trans. Commun.*, vol. 52, no. 10, pp. 1722–1732, 2004.
- [37] H. Urkowitz, "Energy detection of unknown deterministic signals," *Proceedings of the IEEE*, vol. 55, no. 4, pp. 523–531, 1967.
- [38] V. Kuppusamy and R. Mahapatra, "Primary user detection in OFDM based MIMO cognitive radio," in *3rd Int. Conf. on Cognitive Radio Oriented Wireless Netw. and Commun. (CrownCom 2008)*, 2008, pp. 1–5.
- [39] J. Watt, R. Borhani, and A. K. Katsaggelos, *Machine Learning Refined: Foundations, Algorithms, and Applications*, 2nd ed. Cambridge: Cambridge University Press, 2020.
- [40] A. Haddad, D. Slimani, A. Nafkha, and F. Bader, "Users' power multiplexing limitations in NOMA system over gaussian channel," in *2020 8th Int. Conf. on Wireless Netw. and Mobile Commun. (WINCOM)*, 2020, pp. 1–7.
- [41] J. Karedal, N. Czink, A. Paier, F. Tufvesson, and A. F. Molisch, "Path loss modeling for vehicle-to-vehicle communications," *IEEE Trans. Veh. Technol.*, vol. 60, no. 1, pp. 323–328, 2011.
- [42] S. M. Kay, *Fundamentals of statistical signal processing: volume II detection theory*. Prentice Hall, 1998.
- [43] J. G. Proakis, *Digital Communications, 4th Ed.* McGraw–Hill, 2001.